Indian Journal of Chemical Technology
Vol. 32, March 2025, pp. 161-175
DOI: 10.56042/ijct.v32i2.15397

Novel molasses-grafted poly(sodium acrylate) hydrogel: A sustainable solution for water retention and controlled dinotefuran release

Manu Nandal, Vaishali Prashar, Mukul Bansiwal, Ishita Kapoor, Tushar Kansal & Rajinder K. Gupta*

Department of Applied Chemistry, Delhi Technological University, New Delhi, India

*E-mail: rkg67ap@yahoo.com

Received 29 November 2024; accepted 12 February 2025

Sugarcane molasses, a byproduct derived from sucrose manufacturing, is a polyphenolic compound with high sugar content. In this study, a novel molasses-grafted poly(sodium acrylate) hydrogel (M-g-SAH) is synthesized via free radical co-polymerization, using potassium persulfate (KPS) as the initiator and N,N'-Methylenebisacrylamide (MBA) as the crosslinker. M-g-SAH is characterized using Fourier-transform infrared spectroscopy (FTIR), X-ray diffraction (XRD), thermogravimetric analysis (TGA), scanning electron microscopy (SEM) and rheometer. Results demonstrated significant structural, thermal, and morphological changes in M-g-SAH compared to the non-grafted control hydrogel (ctrl). Swelling studies in Milli-Q water revealed that M-g-SAH achieved a maximum swelling index of 225.9 g g^{-1}, with swelling behavior influenced by molasses, KPS, and MBA concentrations. The controlled release of molasses from the M-g-SAH is modelled using Korsmeyer-Peppas, Higuchi, and first-order kinetics. M-g-SAH demonstrated a prolonged release of molasses over 39 h, outperforming the ctrl. According to ANOVA results, the addition of molasses proved to be an effective factor in agricultural trials, as the M-g-SAH hydrogel significantly showed improved water retention and reduced evaporation rate compared to ctrl. Additionally, dinotefuran loading and release studies confirmed M-g-SAH's potential as a pesticide carrier, supporting sustained release applications. These properties make M-g-SAH an eco-friendly and versatile material suitable for agricultural applications.

Keywords: Agriculture, Dinotefuran, Hydrogel, Molasses, Pesticide, Release kinetics

Introduction

Hydrogel forms a 3D network structure comprising polymers crosslinked either chemically or physically. Super absorbent polymers as hydrogels, relative to their own mass, can retain and absorb remarkably enormous amounts of water or aqueous solution[1]. Ideal hydrogels have multiple characteristics; they tend to swell with the liquid and keep their shape intact but increase in volume to reach a physical-chemical equilibrium[2,3]; are non-toxic and inexpensive[4], have high durability, biodegradability[5] and re-wettability. Super absorbent hydrogels have been highly promising in agricultural applications by providing maximum water content and releasing nutrients of choice at the desired rate, thereby increasing crop production by manifolds without negatively impacting the environment[6]. Recent research suggests that incorporating polymer hydrogels into agricultural soil can enhance water efficiency by minimizing water loss and improving soil quality[7, 8]. These hydrogels, known for their water-absorbing properties, significantly enhance soil moisture retention, making them a promising solution for optimizing water utilization in agriculture[9]. Additionally, potassium humate has been found to increase the soil's water-holding capacity while promoting plant growth, improving nutrient uptake, and enhancing yield and fruit quality. A study by Sayed et al., conducted in Egypt during the 2015 and 2016 growing seasons on Egazy olive trees (*Olea europaea* L.), demonstrated these benefits under water stress conditions[10]. Hydrogel-based pesticides function as controlled-release systems, gradually dispensing fertilizers over time. When fertilizers are incorporated into hydrogels, their release rate is significantly slower—approximately half the rate compared to fertilizers dissolved in water alone[11]. In a study by Xianglin et al., a superabsorbent resin modified with sodium humate was developed using inverse suspension polymerization. This resin exhibited excellent water absorption capacity and slow-release characteristics, which were analyzed by monitoring sodium humate release in distilled water[12]. Hydrogels are synthesized from natural polymers, synthetic polymers, and hybrid compositions. Natural polymer hydrogels have gained considerable interest and have undergone examination and evaluation from various perspectives[13].

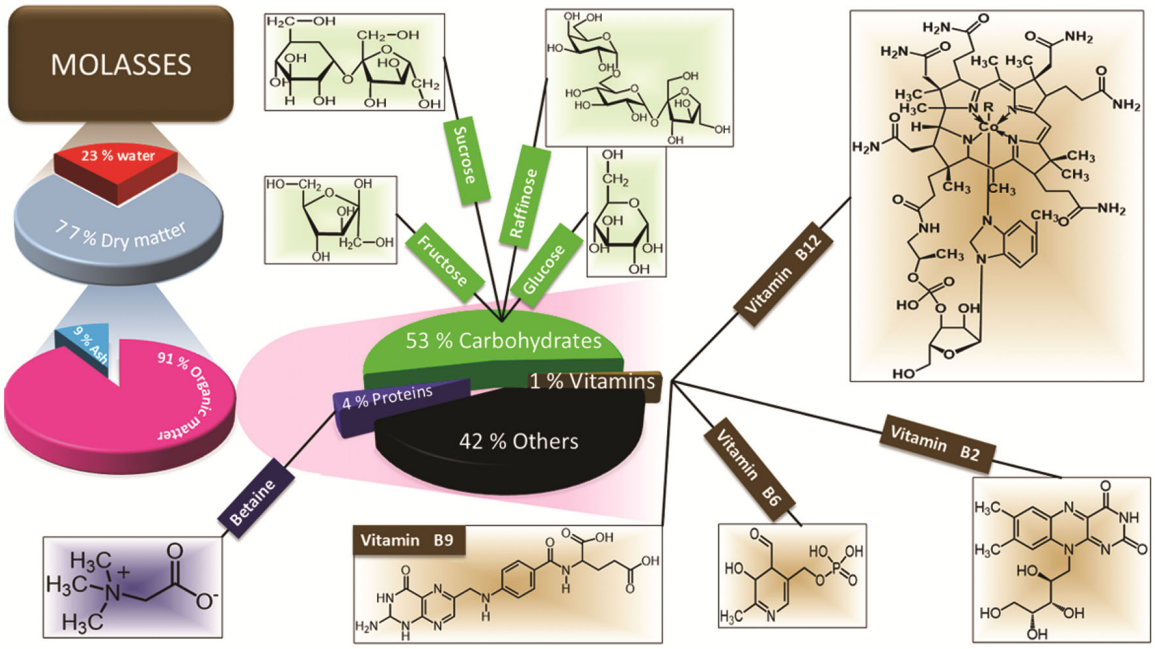

Fig. 1 — Major constituents of cane molasses

Natural biopolymers are commonly employed to prepare "intelligent" hydrogels- ones that show significant changes under the effect of external stimuli. Molasses is a viscous, black-brown effluent obtained in sugar production by repeated crystallization. Sucrose extraction from sugar beets (*Beta vulgaris*) occurs deep in the roots, whereas sugar cane (*Saccharum officinarum*) is derived from the trunk's medullary tissue. The latter comes mainly from South America, Southeast Asia, and the U.S. and is recognized as a high-energy feedstuff owing to its abundance of readily fermentable sugars. Additionally, it contains significant amounts of mineral salts in a bio-accessible form[14]. Fig. 1 shows the chemical composition of cane molasses. It shows that a significant part of molasses is composed of dry matter and serves as a rich source of carbohydrates[15]. Molasses serves as a biodegradable feedstock readily available in adequate amounts to impart antibacterial and antioxidant properties, biodegradable, biocompatible, and nutritional features and no systemic toxicity upon administration[16,17], thereby making it suitable for agriculture and drug delivery. Graft co-polymerization is a well-established and potent method of modifying hydrogels' characteristics, paving the way for adding desired properties and expanding their potential[18]. Hydrogels are typically synthesized by grafting synthetic monomers onto natural polymers. The initiation of radical formation, crucial for polymer growth, is influenced by factors like reaction conditions, solvents, and monomers[19]. Previous studies on molasses have primarily focused on its use as a fermentation feedstock or in the production of biofuels, with limited exploration in polymer chemistry. For instance, Kiselev et al. (2022) investigated the use of sugar beet molasses as a substrate for producing polyhydroxy alkanoates (PHAs) using the bacterium *Cupriavidus necator*. The researchers found that hydrolyzed molasses led to significant biomass and polymer yields, achieving up to 80% polymer yield from bacterial biomass. Similarly, another study explored the use of sugar beet and starch molasses to produce levan, a fructose homopolymer, using *Halomonas sp*. This research showed that pretreated molasses could effectively substitute sucrose, yielding high concentrations of levan. The findings illustrate the versatility of molasses in producing biopolymers, although still within the fermentation context.[20, 21] Another significant study by Fan et al. (2022) integrated sugarcane molasses into lignocellulosic ethanol production, improving fermentation efficiency and increasing ethanol concentrations. The highest ethanol concentration achieved was 94.20 g L^{-1} when molasses was co-fermented with pretreated sugarcane bagasse, showcasing the advantages of using molasses in enhancing biomass resource utilization[22].

Thus, despite its potential, the use of molasses, particularly in hydrogel formation, remains underexplored. This study uses a free radical co-polymerization technique to synthesize and characterize

a novel molasses-grafted poly(sodium acrylate) (M-g-SAH) hydrogel. The incorporation of molasses into the hydrogel is hypothesized to improve its swelling capacity, water retention, and biodegradability, making it particularly suitable for agricultural applications. The structural, thermal, and morphological properties of the M-g-SAH hydrogel are investigated and compared to those of ctrl. The hydrogel's swelling behavior and dinotefuran release kinetics are also examined to evaluate its potential as a water-retention material and a controlled-release system for agrochemicals. The results of this study could provide valuable insights into the development of sustainable hydrogels for use in water management and precision agriculture.

Experimental Section

Materials

Cane Molasses, consisting of concentrated sugarcane juice, iron (1.2%), magnesium (0.4%), and calcium (0.3%),was bought through Amazon from Dhampur Green. Methylenebisacrylamide (MBA) and acrylic acid (A.A.) were obtained from CDH Pvt. Ltd., while potassium persulfate (KPS) was sourced from S.D. Fine Chem Ltd. Sodium hydroxide (NaOH) was procured from Qualikems Fine Chem Pvt. Ltd. All solutions used in the experimental analysis were prepared using Milli-Q (M.Q.) water to ensure purity.

Methods

Synthesis of M-g-SAH

M-g-SAH was synthesized using the free radical co-polymerization technique, with KPS and MBA as the initiator and crosslinker, respectively. At room temperature, the 4.24 g NaOH was added to 7 mL acrylic acid. The reaction mixture containing molasses (0.05 to 0.3g), A.A., NaOH, and KPS (0.25 - 0.56 % of the total monomer) was continuously stirred for 2 h. Subsequently, MBA (0.25 – 0.49 % of the total monomer) was added and stirred at 500 rpm for 2 h. The reaction solution was poured into a test tube and placed in a water bath for 30 min at 60°C. After completion of polymerization, the hydrogel was sliced and soaked in M.Q. water for one day (24 h) to separate unreacted chemicals. Finally, the hydrogel was oven-dried at 70°C until weight stability was achieved[23]. A pictorial representation of the synthesis of M-g-SAH is shown in Fig. 2.

Characterization

In order to facilitate the identification and investigation of the presence of functional groups in the synthesized hydrogels, infrared spectra were acquired using a Perkin Elmer 2000 FT-IR spectrometer with a resolution of 1 cm over a wave number range of 4000 cm^{-1} to 500 cm^{-1}. The PANalytical X'Pert Pro X-Ray Diffractometer was used for X-Ray Diffraction. The surface analysis of the sample was done through SEM, which was carried out on JEOL Japan JSM 6610LV, having two modes, high and low vacuum with electron sources as Tungsten with a voltage range of 1-20 kV and magnification of 1500 and resolution 10 µm. Thermogravimetric Analysis (TGA) was performed using a Perkin Elmer Thermogravimetric Analyzer, TGA 4000, in a nitrogen-controlled atmosphere. The heat was kept constant at 10 °C/min throughout the analysis.

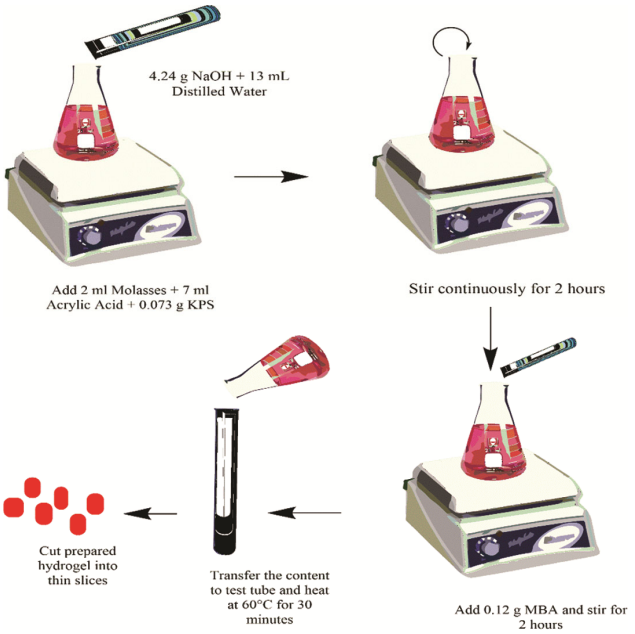

Fig. 2 — Pictorial representation for synthesis of M-g-SAH

Equilibrium Swelling Index

The swelling index of hydrogels, indicative of their water absorption capability, is quantified as the amount of water absorbed. The technique used to evaluate the swelling study of M-g-SAH is well-established and documented in earlier research. The samples under investigation were dried at 50°C until all moisture was eliminated, then weighed and placed in distilled water at room temperature. The samples were weighed at predetermined intervals after being cleaned with filter paper to remove excess water. [24, 25] The swelling index was defined using the Eq. 1.[26]

$$\text{Equilibrium Swelling Index } (gg^{-1}) = \frac{w_s - w_d}{w_d} \quad \ldots(1)$$

Table 1 — Various formulations used in the synthesis of M-g-SAH

Formulation	Molasses (g)	NaOH	KPS (%)	A.A. (mL)	MBA (%)	Equilibrium Swelling index (gg^{-1})	Gel Content (%)
M-g-SAH 1	0.1	8.07	0.25	7.1	0.25	219.73	64.23
M-g-SAH 3	0.1	8.07	0.25	7.1	0.33	183.8	69.62
M-g-SAH 4	0.1	8.07	0.25	7.1	0.41	169.46	73.12
M-g-SAH 2	0.1	8.07	0.25	7.1	0.49	147.28	78.65
M-g-SAH 5	0.1	8.07	0.25	7.1	0.33	184.72	68.21
M-g-SAH 6	0.1	8.07	0.33	7.1	0.33	212.64	64.52
M-g-SAH 7	0.1	8.07	0.41	7.1	0.33	201.33	67.12
M-g-SAH 8	0.1	8.07	0.49	7.1	0.33	189.75	68.34
M-g-SAH 9	0.1	8.07	0.56	7.1	0.33	174.63	71.43
M-g-SAH 10	0.05	8.07	0.25	7.1	0.41	157.56	76.34
M-g-SAH 11	0.1	8.07	0.25	7.1	0.41	163.97	74.63
M-g-SAH 12	0.2	8.07	0.25	7.1	0.41	188.31	69.12
M-g-SAH 13	0.3	8.07	0.25	7.1	0.41	225.9	63.82

where w_s= swollen hydrogel's weight and,w_d= dried hydrogel's weight.

The hydrogel chemical composition, specifically the presence of hydrophilic or hydrophobic groups, also affects their swelling behaviour. The feed composition, including factors such as the changes in concentrations of the crosslinker, initiator, and biopolymer, additionally impacts the swelling ratio. [25]Therefore, the compositions of M-g-SAH varied accordingly, as shown in Table 1.

Gel content determination

The fraction of weight that is insoluble in water is called gel. The soluble fraction of the gel is extracted in boiling water for 24 h with the Soxhlet equipment to determine the gel content. The swollen hydrogels were removed from the apparatus and oven-dried at 50°C. Eq. 2 was used to calculate the gel content of the hydrogel.[27]

$$\text{Gel content (\%)} = \text{SI} = \frac{M_E}{M_I} x100 \quad \ldots(2)$$

M_I is the initial dry weight of hydrogel, and M_E is the final weight of hydrogel after soxhlet extraction.

Measurement of the highest water-retention capacity (W.R.)

This study was conducted on the garden soil of Delhi Technological University, Delhi (28°45'01.9"N 77°07'01.5"E). The moisture content of the soil samples was removed by oven drying for 48 h at 60°C. Then, it was sieved to ensure particle size was less than 30 mesh. The sieved soil samples were then integrated with hydrogel powder up to a concentration of 1% (w/w). The soil-hydrogel mixture was filled into a hollow polypropylene cylindrical tube with a diameter of 5 cm. The bottom of the tube was covered with a nylon cloth, referred to as W_1. A control tube containing soil mixed with non-molasses grafted hydrogel (ctrl) was prepared for comparison. To each tube, 2 mL of M.Q. water was gradually added until it began to seep out from the bottom (W_2). The water addition was repeated every 4 hours to assess the water retention behavior across all samples [28].

Measurement of the Water Evaporation Ratio (WER)

A water evaporation test was conducted for M-g-SAH-treated soil over 55 days. Different sets of hydrogel-treated soil were prepared using oven-dried soil, which had been subjected to drying at 60°C for 48 h. A polypropylene tube was filled with soil, a dried M-g-SAH hydrogel disc, and 50 mL M.Q. water (marked as M_i). The tube, which consisted of ctrl hydrogel, served as a ctrl. The tubes were placed at room temperature and weighed at fixed intervals of 24 h (M_t). WER was determined using Eq. 3.[29]

$$\text{WER} = \frac{(M_i - M_t)}{M_t} x\ 100 \quad \ldots(3)$$

In vitro loading and release of dinotefuran

Dinotefuran was added to the hydrogel by immersing a pre-weighed dry M-g-SAH in dinotefuran solution (2000 ppm) for 24 h. The swollen gels were then withdrawn from the water and oven-dried until a consistent weight was reached.

The dinotefuran released from M-g-SAH was estimated by placing oven-dried, dinotefuran-loaded samples in a beaker containing 100 mL of M. Q water at ambient temperature. Samples for measuring the concentration of released dinotefuran were withdrawn at predetermined intervals while the same volume of M.Q. water was supplemented back to the beaker to maintain a constant volume. The absorbance of the supernatant was measured at 270.5 nm by a UV–

visible spectrophotometer. A standard calibration curve was obtained using Eq. 4 and then applied to determine the concentration of dinotefuran.

$$C\ (ppm) = \frac{A-0.4125}{0.0032} \quad \ldots(4)$$

Where, C represents the dinotefuran concentration in the water sample and A is the UV-visible absorbance of the solution of unknown concentration.

Determination of loading efficiency of dinotefuran

The amount of dinotefuran loaded into the M-g-SAH hydrogel formulations was determined by calculating the difference between the initial dinotefuran and the concentration of free dinotefuran in the corresponding supernatant. This analysis was performed using a UV–Vis spectrophotometer (Shimadzu UV-Spectrophotometer, UV-1800) at a wavelength of 254 nm. Subsequently, a standard curve was utilized to convert the absorbance readings of the samples into dinotefuran concentrations. The loading efficiency (L.E.) of dinotefuran was calculated using Eq.5.[30]

$$LE\ (\%) = \frac{A_{total}-B_{free}}{A_{total}} \text{x } 100 \quad \ldots(5)$$

Where A_{total} is the amount of dinotefuran used to prepare M-g-SAH, and B_{free} is the amount of freely present dinotefuran in the supernatant.

Results and Discussion

Mechanism for the synthesis of M-g-SAH

The KPS initiator generated anionic radicals, which facilitated the formation of phenoxy radicals on molasses. Subsequent reactions of these active radicals with the vinyl groups of sodium acrylate led to the propagation of poly(sodium acrylate) chains. According to Ganguly et al., the divinylic monomer N,N'-methylenebisacrylamide (MBA), incurs interchain covalent crosslinking due to its multifunctional character. Consequently, the poly(sodium acrylate) chains propagated through further cross-linkage until crosslinking occurred between the polymer chains, with MBA as the crosslinker and terminating the process to form M-g-SAH. The electrostatic repulsion between negatively charged carboxylate ions in the poly(sodium acrylate) polymer chains causes network expansion, enhancing the hydrogel's water absorption capacity.

All synthesized hydrogels' swelling behavior and gel content were evaluated in M.Q. water, as summarized in Table 1. Notably, M-g-SAH 13 exhibited the highest swelling capacity among the samples. Due to its superior performance, M-g-SAH 13 was selected for further experimental analysis and detailed studies.

The gel content percentage of hydrogels varied according to the concentration of crosslinker, biopolymer, and initiator. The gel content showed an inverse relation with the swelling of hydrogels, primarily determined by the degree of crosslinking. Increased crosslinking generally leads to a higher gel fraction, which can restrict the mobility of polymer chains. This restriction often results in decreased swelling capacity because the network becomes less flexible, limiting the amount of water absorbed [31]. Gel contents of synthesized hydrogels were found in between 64 - 76 %.

Characterization

FT-IR

The FTIR spectra of the Ctrl and M-g-SAH samples are presented in Fig. 3(a) and 3(b), respectively, as a comparative analysis to elucidate the functional group variations and structural

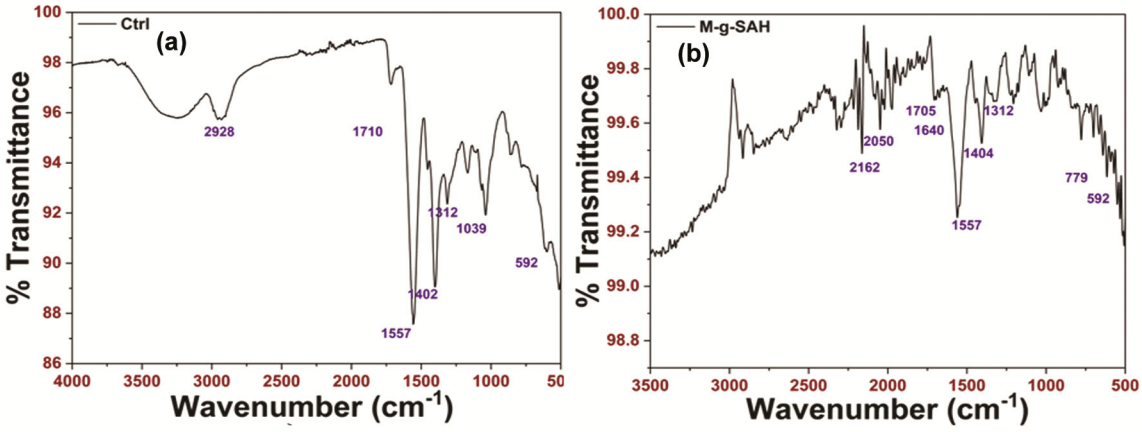

Fig.3 — FTIR spectra of (a) Ctrl and (b) M-g-SAH

characteristics of the materials under investigation. Ctrl has a band around 2928 cm^{-1} owing to the -CH stretching in $-CH_2$ or $-CH_3$ groups. A peak at 1312 cm^{-1} confirms the presence of C-N. The C=O stretching vibration, localized at approximately 1710 cm^{-1}suggests that the carboxylic acid functionalities are present within the matrix[32]. The low-frequency bands around 590 cm^{-1} indicate skeletal vibrations of the polymer backbone.

The significant water content in molasses affects the FT-IR spectrum. The O-H stretching vibrations from water molecules generally show a broad, strong absorption band around 3400 cm^{-1}, and the bending vibrations of water appear near 1640 cm^{-1}. The carboxyl group (-COOH) shows strong stretching vibrations between 1700–1740 cm^{-1}. Phenolic hydroxyl groups also contribute to bands around 3000–3500 cm^{-1} (O-H stretch). Molasses is rich in sugars such as sucrose, glucose, and fructose. These compounds display absorption bands primarily in the 1000–1200 cm^{-1} region, corresponding to C-O stretching vibrations in the carbohydrate structure. The band at 1039 $cm^{-1}$is linked to C-O-C vibrations due to the glycosidic linkages present in carbohydrates of molasses[33]. Peaks between 1620–1650 cm^{-1} may indicate the presence of conjugated or aromatic compounds in molasses.

The presence of two prominent peaks in both ctrl and M-g-SAH at 1557 cm^{-1} and 1402 $cm^{-1}$is associated with the carboxylate anion's vibration[34]. The broad spectrum and a peak at 1312 cm^{-1} and 592 cm^{-1}, respectively, indicate the presence of the C-N and O=C–N groups of MBA[35]. The stretching vibrations associated with C≡C and C≡N bonds exhibit absorption bands typically ranging from 2050~2200 cm^{-1}. In M-g-SAH, the 2162 cm^{-1} and 2050 cm^{-1} peak show weak terminal ≡C-H stretch. A medium to weak intensity level characterizes these bands. The M-g-SAH exhibits new peaks around 2162 cm^{-1} and 2050 cm^{-1}, which are absent in the ctrl. These peaks suggest the successful grafting of molasses onto the hydrogel network, likely introducing new unsaturated bonds or carbonyl groups. The overall similarity in the main COO^- peaks (1557 cm^{-1} and 1404 cm^{-1}) between both spectra confirms that the basic hydrogel structure is retained, while the grafting modifies certain chemical characteristics.

SEM

The SEM images of the Ctrl hydrogel sample and the M-g-SAH sample, both at a magnification of 1500x, are shown in Fig. 4. The ctrl hydrogel surface is even and smooth with some cracks which have been caused by oven drying. On the contrary, the structure of the M-g-SAH sample shows granular, uneven, porous and crosslinked morphology. This significant difference in morphology suggests that the grafting process and incorporation of molasses have dramatically altered the material's structure. The M-g-SAH sample demonstrates much higher porosity compared to the ctrl. The observed properties facilitate the adsorption of more water by molasses-grafted hydrogel in comparison to ctrl hydrogel[36].

XRD

The XRD patterns of the Ctrl and M-g-SAH samples (Fig. 5) are shown in the 2θ range 5°-90°. The M-g-SAH and Ctrl samples exhibited two complex and broad peaks within a specific range, with their peak maxima at 18° and 32°, respectively. The detected maxima in the XRD patterns indicate an amorphous polymer structure, suggesting that the material lacks long-range order and exhibits a disordered arrangement of its constituent polymer chains[25, 37]. The ctrl hydrogel shows a slightly higher

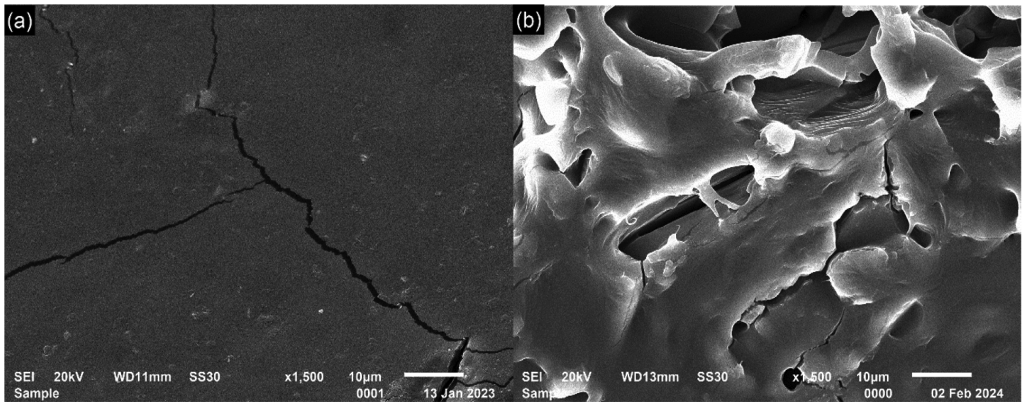

Fig. 4 — SEM images of (a) Ctrl sample and (b) M-g-SAH

intensity and broader peak than the molasses-grafted hydrogel M-g-SAH. The lower intensity of the M-g-SAH sample suggests that incorporating molasses has reduced the overall crystallinity or order within the hydrogel structure, possibly due to the interference of molasses components with polymer chain packing [38]. The absence of new sharp peaks in the M-g-SAH sample indicates that the molasses is well-integrated into the hydrogel structure without forming separate crystalline phases. In conclusion, the XRD results indicate that grafting molasses onto the poly (sodium acrylate) hydrogel has caused changes in the polymer structure, likely reducing its overall crystallinity or order without fundamentally altering its amorphous nature.

TGA and DTA

TGA is a quantitative analysis that assesses the mass variations in hydrogels subjected to heating. This technique helps determine thermal stability, degradation temperatures, and identification of distinct weight loss stages within the hydrogel structure. It also establishes different temperature ranges for different thermal events[39]. Analysis of the thermogram for the M-g-SAH sample, as shown in Fig. 6 (a and b), indicates that both materials show a gradual weight loss as temperature increases. Three distinct weight loss intervals are found within the temperature range of 40-780°C. In the case of M-g-SAH, the initial loss of weight of 24.54% within the temperature range of 40-420°C can be associated with the release of moisture inherently present in the polymeric structure. Subsequently, the temperature interval of 430-580°C is characterized by the onset of sample decomposition, accounting for a weight loss percentage of 23.5%. The third and final stage, incorporating the temperature spectrum of 600-780°C, is linked with the decomposition of the primary polymeric backbone, resulting in a weight loss of 9.55% [40]. The residual mass of M-g-SAH and ctrl were found to be 41.87 and 33.21 %, respectively.

The DTG graph in both samples shows an endothermic event (downward peak) in this range of 0-200°C. However, the ctrl has a sharper, deeper peak around 100°C, indicating a more rapid moisture loss. The M-g-SAH sample shows a broader, shallower peak, suggesting a more gradual moisture loss, possibly due to more vital water binding from the molasses components. Both samples exhibit a prominent endothermic peak centered around 450°C, representing the primary decomposition of the poly sodium acrylate backbone. The maximum degradation was observed at 338°C and 450°C for M-g-SAH and ctrl, respectively.

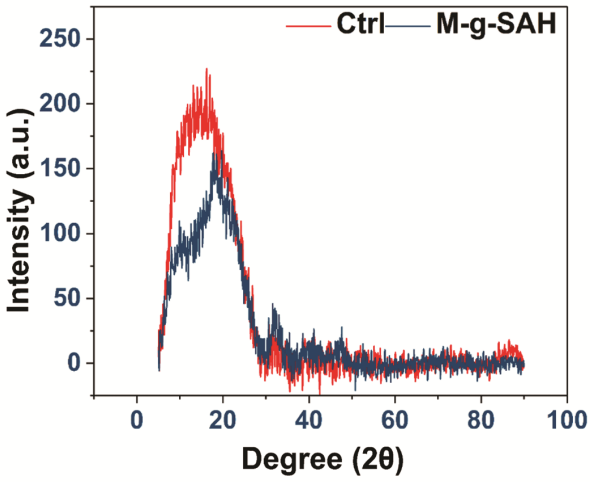

Fig. 5 — XRD plots of Ctrl and M-g-SAH

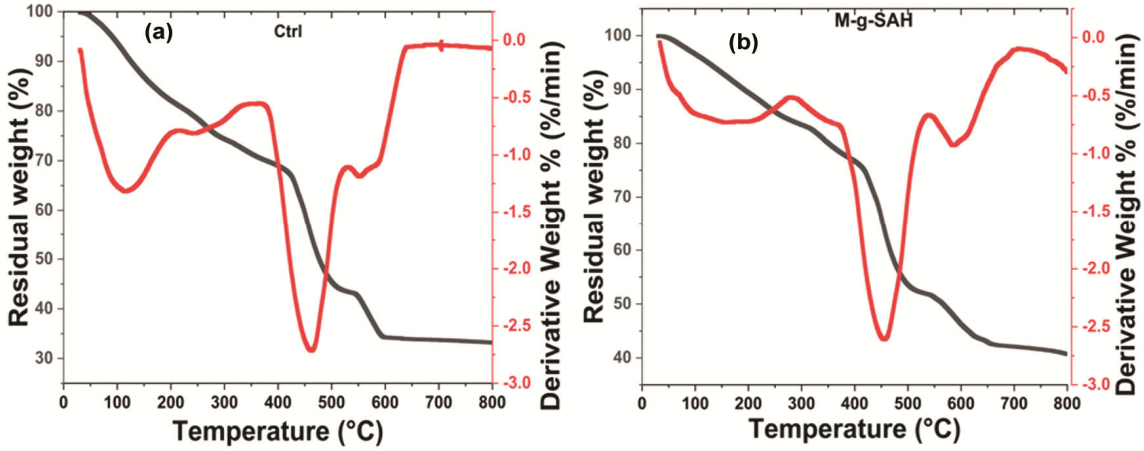

Fig. 6 — TGA and DTA plot of (a) Ctrl and (b) M-g-SAH

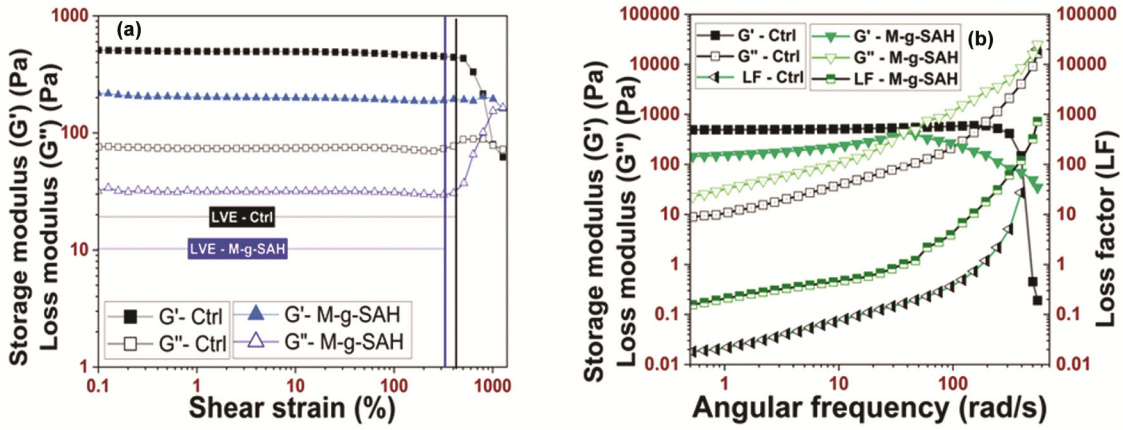

Fig. 7 — Rheological analysis of M-g-SAH and ctrl: (a) amplitude sweep and (b) frequency sweep

Table 2 — Frequency sweep rheological analysis data of M-g-SAH and ctrl hydrogels

Sample	Frequency Region up to cross-over point			Cross-over point	Frequency region after cross-over point		
	Storage modulus G' (Pa)	Loss modulus G" (Pa)	Loss Factor Tan θ	Angular frequency (rad/s)	Storage modulus G' (Pa)	Loss modulus G" (Pa)	Loss Factor Tan θ
M-g-SAH	144.94	22.74	0.156	37	34.62	24876	728.54
Ctrl	491.08	8.89	0.018	194	0.453	9063.7	200081

In conclusion, the molasses-grafted poly(sodium acrylate) hydrogel demonstrates improved thermal stability compared to the non-grafted ctrl, retaining more of its initial weight across the studied temperature range. It suggests that adding molasses to the hydrogel enhances its resistance to thermal decomposition.

Rheology

Rheological studies provide insights into the relationship between the chemical structure of hydrogels and their macroscopic behaviour.[41] The rheological properties of the synthesized hydrogels were compared with ctrl to investigate the effect of molasses in the hydrogels, as shown in Fig. 7(a) and 7(b).

During the amplitude sweep test, the shear stress amplitude was varied at a constant frequency of 10 rad/s. At low strain, both the loss modulus (G") and storage modulus (G') remained stable, indicating that the hydrogel's structure was unaffected. This phase, known as the linear viscoelastic region (LVE), represents the range in which the hydrogel maintains its structural integrity under applied deformation. However, the consistency between G" and G' decreased with a further increase in strain. This deviation from the consistent modulus indicates structure disruption and the LVE region's termination.

Both M-g-SAH and Ctrl show higher storage modulus (G') than loss modulus (G") across most of the strain range, indicating predominantly elastic behaviour. M-g-SAH exhibits lower G' and G" values compared to Ctrl, suggesting it is softer and less rigid. However, M-g-SAH has a broader LVE region, indicating that the grafted hydrogel retains elasticity over a more comprehensive strain range than the ctrl.

During the frequency sweep test, the frequency was varied from 0.1 to 500 rad/s, while the shear strain percentage was maintained constant within the linear viscoelastic (LVE) region. It was observed that at higher frequencies, the loss modulus (G") dominated, whereas, at lower frequencies, the storage modulus (G') was more prominent, indicating a viscoelastic solid behaviour. The parameter Tan θ (dimensionless), representing the ratio of the loss modulus to the storage modulus, typically ranges from 0 to 1 for viscoelastic materials. For purely viscous behaviour, Tan θ approaches infinity, corresponding to a phase angle (θ) of 90°, while for ideal elastic behavior, Tan θ equals 0, corresponding to a phase angle of 0°.[42]

From Table 2, the ctrl has a higher initial G' (491.08 Pa), suggesting a more solid-like structure at lower strains. M-g-SAH has a lower initial G', but the significant increase after the cross-over point suggests a strengthening of the elastic network at higher frequencies. M-g-SAH has a higher loss factor (tan θ) before the cross-over point (0.156), indicating more viscous behavior than the ctrl. Ctrl has a much lower tan θ (0.018) before the cross-over, suggesting it is

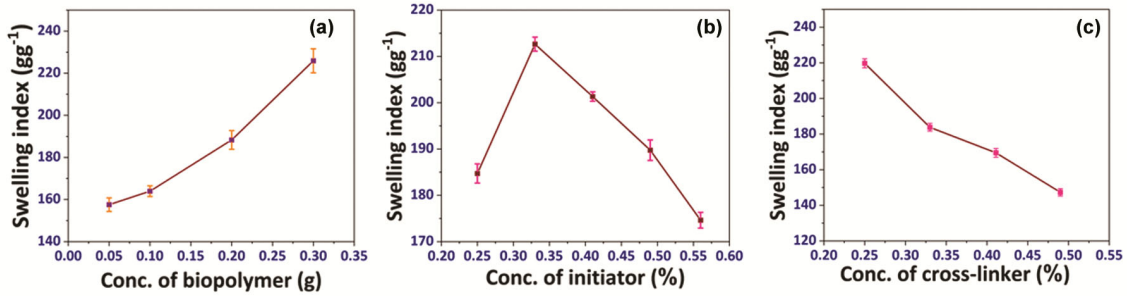

Fig. 8 — Effect of variation of (a) biopolymer (Molasses), (b) initiator (KPS) and (c) crosslinker (MBA) on the swelling index.Error bars represent standard deviation

more elastic even at lower strains. Thus, M-g-SAH hydrogel shows superior performance in terms of elasticity at higher frequencies and more extensive strain ranges, indicating that the molasses grafting enhances the elastic nature of the hydrogel.

Ctrl hydrogel displays more stable solid-like properties in the lower frequency and strain regions but lacks strength at higher frequencies and strains, as indicated by the rapid increase in G" after the cross-over.

Swelling study

a) Influence of Biopolymer on the Degree of Swelling

The concentration of a biopolymer significantly affects the swelling properties of hydrogels. An increment in the concentration of molasses from 0.05 to 0.3g enhances swelling ability from 157.56 to 225.9 $g\,g^{-1}$, shown in Fig. 8(a). The higher concentration of molasses affects crosslinking, resulting in a loose structure[31,43]. Additionally, the diverse hydrophilic groups in molasses offer more opportunities for water molecules to interact, improving the swelling behaviour of hydrogels. These combined effects contribute to the improved swelling behaviour of hydrogels with increased molasses concentration.

b) Influence of Initiator on the Degree of Swelling

The variation of the swelling ability of M-g-SAH hydrogel by changing KPS content is depicted in Fig. 8(b). The swelling ratio is between 184.72 to 174.63 $g\,g^{-1}$ is obtained when KPS content varies from 0.25 to 0.56 %. The higher KPS concentration results in an upsurge in free radical production. An escalation in free radical quantities leads to an accelerated rate of polymerization process. As a result, the polymer chains in the network become more extensive, with a reduction in the average kinetic chain size[23]. This alteration in the network configuration may result in a structure with increased porosity and a higher swelling index. The optimal water absorption occurred at 0.33% of the initiator. Higher initiator concentrations exceeding 0.33% might accelerate reaction velocity, reverting to lowering the hydrogel's network space, which, consequently, may reduce the hydrogel's swelling index.

c) Influence of Crosslinker on the Degree of Swelling

The porous morphology, swelling behaviour, and mechanical integrity of M-g-SAH depend upon the concentration of crosslinking agent (MBA). By adjusting the degree of crosslinking, a molasses-based hydrogel with desired properties can be prepared, providing a versatile platform for designing and customizing pesticide delivery systems. The swelling ratio of the prepared sample decreased from 219.73 to 147.28 g g^{-1} when the amount of crosslinking agent was raised from 0.25 to 0.49 %, as depicted in Fig. 8(c).The cutback observed in water absorption is linked to the generation of a denser structure caused by increased crosslinking, which is associated with a lower water absorption capacity[44]. When the concentration of MBA falls below 0.25%, the graft reaction is ineffective, producing gel-like material with inadequate dimensional stability[28]. MBA enhances crosslinking, decreasing the available free volume within the polymer network, resulting in reduced swelling behaviour of the hydrogel.

Agricultural applications of M-g-SAH

Highest water retention capacity

Water availability in the soil is of utmost importance for better plant growth. Fig. 9 shows the water retention capacity of two hydrogels, M-g-SAH and Ctrl, at different concentrations. Both hydrogels show an increase in water absorption as their concentration increases. The rate of increase is steeper

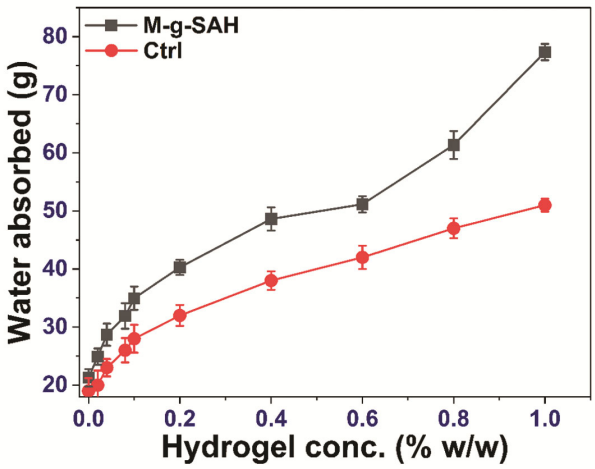

Fig. 9 — Highest water retention capacity of (a) Ctrl and (b) M-g-SAH. Error bars represent standard deviation

at lower concentrations (0-0.2%) and more gradual at higher concentrations. Still, M-g-SAH consistently demonstrated higher water absorption capacity than the ctrl at all concentrations. This superior performance is consistent across all tested concentrations (0-1% wt/wt), with the difference becoming more pronounced at higher concentrations. The improved water retention of M-g-SAH indicates that the molasses grafting process successfully modifies the hydrogel structure, likely increasing its hydrophilicity or creating more water-binding sites. This enhanced water retention property makes M-g-SAH a promising material for applications in agriculture, particularly in water-scarce regions, where it could help to improve soil moisture retention and reduce irrigation requirements.

Water Evaporation Ratio

The water evaporation test, conducted over 55 days, indicates similar trends between the M-g-SAH-treated soil and the ctrl hydrogel-treated soil, as depicted in Fig. 10. The M-g-SAH-treated soil exhibits notably enhanced water retention, characterized by a significantly slower evaporation rate and a more gradual increase in water loss throughout the test period. By the end of the 55 days, the M-g-SAH-treated soil had reached approximately 85% water evaporation. In contrast, the ctrl hydrogel-treated soil showed a steady increase in water evaporation, with around 75% water loss by day 55, likely due to the interaction between water and polymer molecules, along with the macromolecular network hindering evaporation. [29]

Notably, as time progressed, the performance gap between M-g-SAH and the ctrl hydrogel widened,

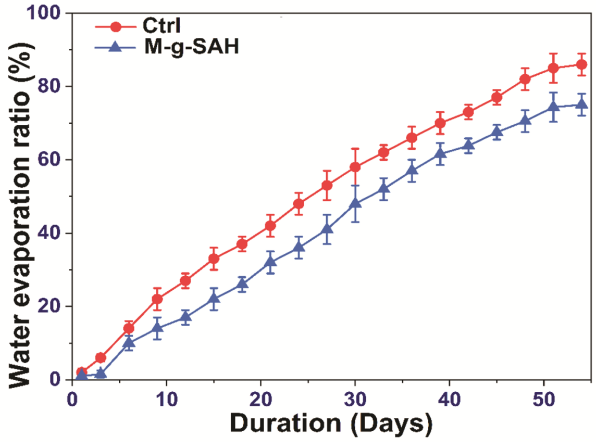

Fig. 10 — Water Evaporation study plots of (a) Ctrl and (b) M-g-SAH. Error bars represent standard deviation

highlighting the superior long-term water retention capabilities of M-g-SAH.

These findings are consistent with swelling study data, where M-g-SAH demonstrated higher swelling capacity than the ctrl hydrogel. The extended duration of water retention after hydrogel application suggests that water can remain in the soil for a longer period, offering plants more time to absorb water. This feature is especially beneficial during extended dry periods or under stress conditions, potentially enhancing plant growth. [45]

The results of the ANOVA (Table 3) revealed a significant difference in water evaporation ratios, water evaporation ratio and amount of dinotefuran released by M-g-SAH and the ctrl hydrogel, as indicated by an observed P-value (F-test) smaller than 0.05. This suggests that the changes observed in the following experiments were not due to random measurement errors but rather to the addition of molasses in hydrogel synthesis.

Dinotefuran Loading Efficiency

An ideal hydrogel used for release application should have good loading efficiency and allow for release over a longer time. The loading efficiency of synthesized dinotefuran-loaded hydrogels M-g-SAH13 and ctrl were found to be 63.52% and 57.44%, respectively.

Release Kinetics of Dinotefuran

The dinotefuran release process from all formulations followed a gradual mechanism. Initially, water penetrates the hydrogel, causing it to swell as it absorbs water. This absorption continues until a dynamic equilibrium is established between the

Table 3 — ANOVA table for conducted experiments

Source	Sum of squares	DF	Mean square	F-Value	P-value
Water Retention Ratio	845.60	3	547.34	110.23	2.67×10^{-3}
Water Evaporation	657.24	3	385.45	97.22	3.78×10^{-2}
Dinotefuran release	256.56	3	220.40	6.45	4.22×10^{-2}

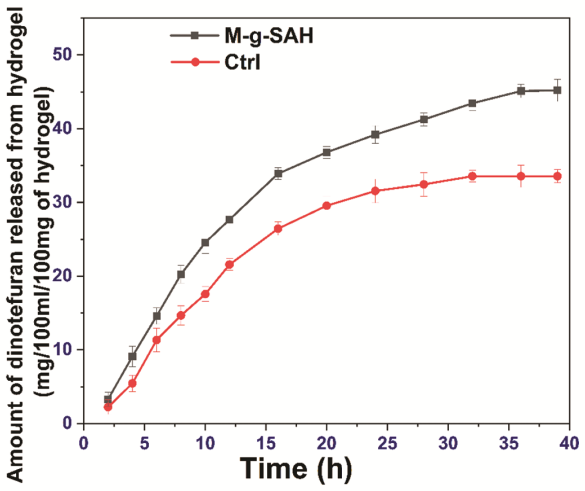

Fig. 11 — Amount of Dinotefuran released from M-g-SAH and Ctrl.Error bars represent standard deviation

hydrogel's free water and the beaker's water. During this phase, the dinotefuran embedded within the hydrogel matrix dissolves and diffuses. The release of dinotefuran into the water occurs due to osmotic pressure differences and the ongoing dynamic exchange of free water between the hydrogel and the environment [29].

The release kinetics of dinotefuran from M-g-SAH and ctrl was observed in M.Q. water. It was found that M-g-SAH and ctrl released dinotefuran for 39 and 32 h, respectively. The amount of dinotefuran released was observed to be 45.2 mg and 33.56 mg for M-g-SAH and Ctrl, as shown in Fig. 11. The disparity in released dinotefuran is attributed to the presence of molasses in the hydrogel.

The Korsmeyer-Peppas model, first order and Higuchi model are employed to describe the release mechanism of dinotefuran from M-g-SAH and ctrl hydrogels (Fig. 12). Korsmeyer Peppas model is described by the Eq. 6.[26]

$$\frac{M_t}{M_\infty} = k_{kP}t^n \quad ...6$$

Where, M_t represents the concentration at a particular time and M_∞ represents the concentration at the equilibrium point.

This model shows the release behaviour only for the first 60% of the release of the pesticide[46]. The ratio of M_t to M_∞ represents total molasses in fraction released in time 't', while 'k' is a constant related to the polymer structure. The 'n' value indicates the deviation from Fickian behaviour, and it helps characterize the nature of the diffusion process in systems exhibiting non-Fickian or anomalous diffusion. If the value of 'n' is > 0.45, it suggests a diffusion-controlled release mechanism governed by Fickian diffusion. On the other hand, when the value of 'n' lies in the range of 0.45 to 0.89, it indicates a non-Fickian transport mechanism. If the value of 'n 'equals 0.89, it indicates zero-order release (Case II Transport). When the value of 'n' exceeds 0.89, it is classified as super case II transport[26].The coefficient of determination (R^2) value represents the model's accuracy, ranging from 0-1. A value over 0.95 references the model to be accurate.

The Weibull model can be represented using Eq. 7.[26]

$$\{\log(-\ln(1-m)\}=\beta\log(t-Ti)-\log\alpha \quad ...(7)$$

Where, m is the amount of pesticide dissolved as a function of time t, β=shape parameter, α=scale parameter, Ti=Location parameter/time lag usually zero, t=Time in h. The α-value in the Weibull model shows the time scale or apparent rate constant, while the β value characterizes the shape of the curve. When it comes to polymeric matrices, the exponent β is a marker for the pesticide's method of transport across the matrix. In fractal and Euclidian spaces, Fickian diffusion is linked to β values 0.75; on the other hand, β values in the range 0.75-1 are linked to a combined mechanism (Fick diffusion and swelling-controlled transport). For values of β higher than 1, it is demonstrated that the pesticide transport follows a complex release mechanism [47, 48].

The release kinetics of the pesticide, which followed the first order, can be expressed as Eq. 8.[23]

$$\frac{dC}{dT} = -Kc \quad ...(8)$$

Where K is the first order rate constant expressed in units of time^{-1}.

Eq. 8 can be expressed as $\log C = \log C_0 - Kt/2.303$

where C_0 is the initial concentration of the pesticide, k is the first-order rate constant, and t is the time[49]. The data obtained are plotted as a log

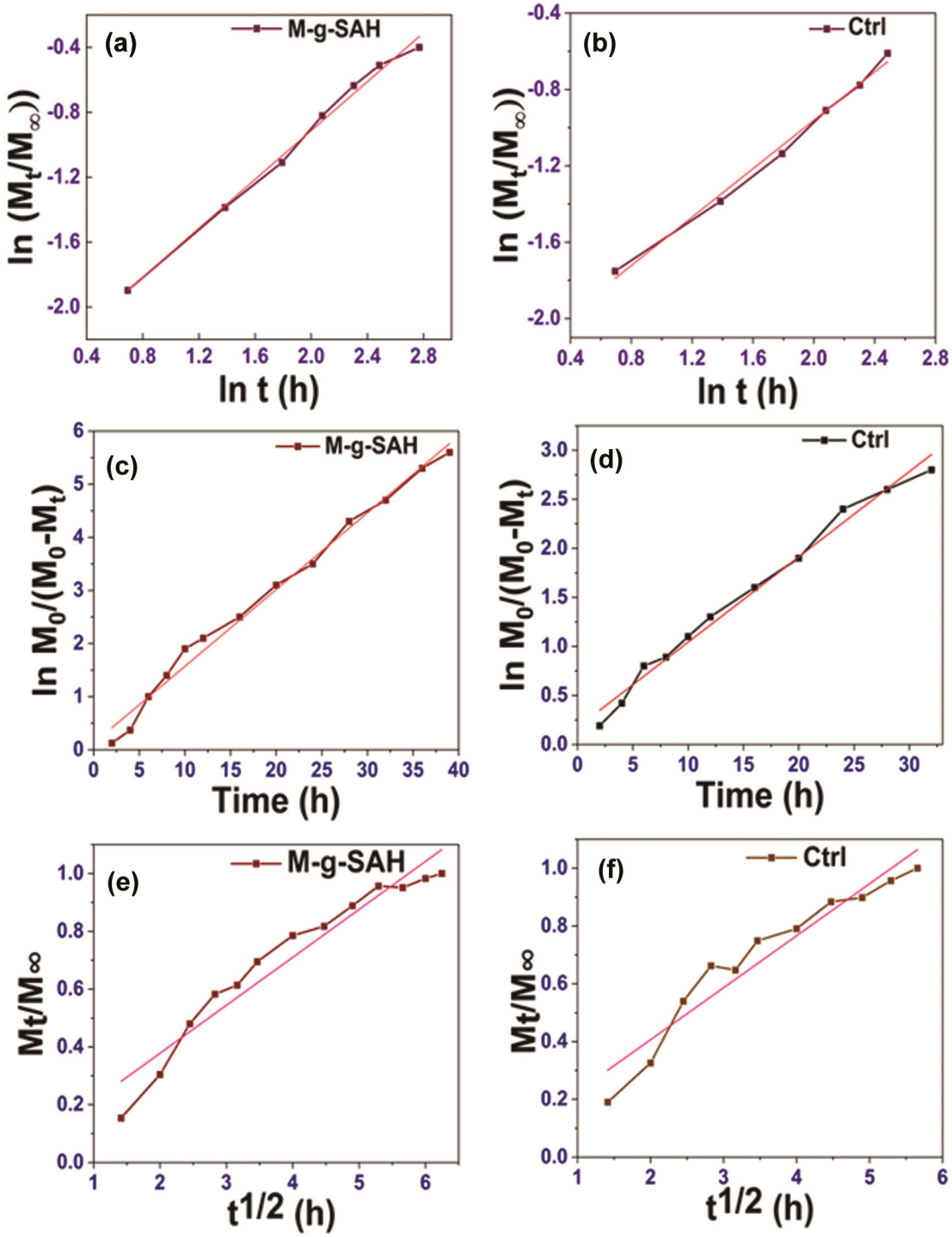

Fig. 12 — Dinotefuran release kinetics using (a) Korsmeyer Peppas Method– M-g-SAH, (b) Korsmeyer Peppas Method- Ctrl, (c) Higuchi model- M-g-SAH (d) Higuchi model- ctrl, (e) First order model- M-g-SAH and (f) First order model- ctrl

cumulative percentage of pesticide remaining vs. time, yielding a straight line with a slope of -K/2.303.

Table 4 shows the R^2 and relevant parameters for the Korsmeyer-Peppas, First Order, and Higuchi model, comparing the M-g-SAH with a Ctrl hydrogel. The 'n' values for both formulations in the Korsmeyer-Peppas Model fall between 0.45 and 0.89 (0.822 for M-g-SAH and 0.764 for ctrl), indicating their anomalous transport (non-Fickian diffusion).

Table 4 — Mathematical models used for the study of release kinetics of dinotefuran

Model	Formulation	R^2	Parameter
Korsmeyer Peppas	M-g-SAH	0.9932	n= 0.822 k=0.468
	Ctrl	0.9956	n= 0.764 k=0.593
First order	M-g-SAH	0.9884	k=0.134
	Ctrl	0.9863	k=0.162
Higuchi	M-g-SAH	0.9387	k=19.452
	Ctrl	0.9278	k=21.614

The higher 'n' value for M-g-SAH suggests a more significant contribution of polymer relaxation/erosion in the release process, possibly due to the molasses grafting. The lower 'k' value for M-g-SAH (0.468 vs 0.593 for Ctrl) indicates a slower initial release rate. The first-order model also demonstrated a good fit for both formulations ($R^2 > 0.98$) but slightly lower than the Korsmeyer-Peppas model. The k value for M-g-SAH (0.134) is lower than the Ctrl (0.162), consistent with the Korsmeyer-Peppas model, indicating a slower release rate for M-g-SAH. The Higuchi Model showed lower R^2 values (0.9387 for M-g-SAH and 0.9278 for Ctrl) than the other models, suggesting that simple diffusion alone does not fully explain the release process. The k value for M-g-SAH (19.452) is lower than the Ctrl (21.614), indicating slower diffusion-controlled release in the modified hydrogel.

Thus, the molasses-grafted hydrogel demonstrates a significantly modified release profile for dinotefuran compared to the ctrl. It exhibits a slower initial release rate and extends the overall release duration from 32 to 39 hours, a 21.9% increase in release time. The combination of slower initial release (lower k values) and longer duration suggests that M-g-SAH provides a more controlled and prolonged release profile.

Conclusion

This study successfully synthesized a molasses-grafted poly(sodium acrylate) hydrogel (M-g-SAH) via free radical co-polymerization, with KPS as the initiator and MBA as the crosslinker. Incorporating molasses, a renewable biopolymer, significantly enhanced the hydrogel's water retention and structural properties. Characterization using FTIR confirmed successful grafting of molasses, while XRD and SEM analyses revealed an amorphous structure and a more porous morphology than the ctrl hydrogel. TGA indicated improved thermal stability, with M-g-SAH retaining 41.87 % of its mass at 800°C, demonstrating superior thermal resistance. The swelling Index of M-g-SAH reached a maximum of 225.9 g g^{-1}. This enhanced swelling behavior was attributed to the higher molasses concentration, which increased the availability of hydrophilic groups. Crosslinker concentrations showed an inverse relationship with swelling, as denser networks restricted water absorption. The hydrogel's gel content ranged from 64% to 76%, reflecting its adjustable crosslinking density. In dinotefuran release studies, M-g-SAH exhibited a sustained release over 39 hours that lasted longer than the ctrl hydrogel (32 h), following non-Fickian diffusion kinetics, as described by Korsmeyer-Peppas and the first-order model. Additionally, dinotefuran loading efficiency was found to be 63.52% which is 10.58% greater than ctrl. In agricultural tests, the hydrogel showed 20% greater water retention than the ctrl, making it highly effective for soil moisture conservation. These results demonstrate that M-g-SAH is an eco-friendly, multifunctional material with great potential for agricultural water management, controlled release systems, and environmental sustainability applications.

Acknowledgements

The authors would like to acknowledge the Institute of Pesticide Formulation and Technology, Gurugram for providing dinotefuran. The authors would also like to thank the Department of Applied Chemistry, Delhi Technological University, Delhi for providing the research facilities.

References

1 Zohuriaan-Mehr MJ, & Kabiri K Superabsorbent polymer materials: A Review, *Iran Polym J*, 17 (2008) 451.

2 Duran S, Şolpan D & Güven O, Synthesis and characterization of acrylamide–acrylic acid hydrogels and adsorption of some textile dyes, *Nucl Instrum Meth Phys Res Sect B Beam Interact with Mater Atoms*, 151 (1999) 196.

3 Kumar J & Purwar R A, Schiff base hydrogel of oxidized okra gum and carboxymethylated chitosan: A biocompatible and biodegradable injectable system for drug delivery in wound care *Colloid Polym Sci*, 302 (2024) 1923.

4 Kumar J & Purwar R, Injectable mesquite gum and carboxymethyl chitosan hydrogel using schiff base crosslinks: a versatile platform for drug delivery in wound care *Macromol Res*, 32 (2024) 1237.

5 Kumar J & Purwar R, Biodegradable, biocompatible, and self-healing, injectable hydrogel based on oxidized Azadirachta indica gum and carboxymethyl chitosan through dynamic imine-linkage for biomedical application, *Iran Polym J*, (2024).

6 Goncalves A A L, Fonseca A C, Fabela I G P, Coelho J F J & Serra A C, Synthesis and characterization of high performance superabsorbent hydrogels using bis[2-(methacryloyloxy)ethyl] phosphate as crosslinker, *Exp Polym Lett*, 10 (2016) 248.

7 Song B, Liang H, Sun R, Peng P, Jiang Y & She D, Hydrogel synthesis based on lignin/sodium alginate and application in agriculture, *Int J Biol Macromol*, 144 (2020) 219.

8 Manu, Kumar D & Gupta R K, Natural polymers-humic acid and lignin based hydrogels: In agriculture, environment and energy storage, *Ind Crops Prod*, 219 (2024) 119029.

9 Prashar V, Nandal M, Gupta R K & Tyagi Y K, Novel Synthesis and application of carboxymethylated cassia fistula -based hydrogel for extended-release of dinotefuran, *ChemSelect*, 9 (2024) e202403421.

10 El-Sayed A E R & Mohamed S, Enhancing olive trees growth and productivity by using hydrogel and potassium humate under rain-fed condition in northern western coastal zone, *Egypt J Desert Res*, 67 (2017) 137.

11 Ghobashy M M The application of natural polymer-based hydrogels for agriculture, *Hydrogels Based Nat Polym*, 12 (2019) 329.

12 Yu X, Wang Z, Liu J, Mei H, Yong D & Li J Preparation, swelling behaviors and fertilizer-release properties of sodium humate modified superabsorbent resin, *Mater Today Commun*, 19 (2019) 124.

13 Peppas N A, Hilt J Z, Khademhosseini A & Langer R Hydrogels in biology and medicine: From molecular principles to bionanotechnology, *Adv Mater*, 18 (2006) 1345.

14 Mordenti A L, Giaretta E, Campidonico L, Parazza P & Formigoni A, A review regarding the use of molasses in animal nutrition, *Animals*, 11 (2021) 115.

15 El-Asri O & Farag M A, The potential of molasses from different dietary sources in industrial applications: A source of functional compounds and health attributes, a comprehensive review, *Food Biosci*, 56 (2023) 103263.

16 Grabek-Lejko D & Tomczyk-Ulanowska K, Phenolic content, anti-oxidant and antibacterial activity of selected natural sweeteners available on the Polish market, *J Environ Sci Heal Part B*, 48 (2013) 1089.

17 Takara K, Ushijima K, Wada K, Iwasaki H & Yamashita M, Phenolic compounds from sugarcane molasses possessing antibacterial activity against cariogenic bacteria, *J Oleo Sci*, 56 (2007) 611.

18 Hu X, Wei W, Qi X, Yu H, Feng L, Li J, Wang S, Zhang J & Dong W, Preparation and characterization of a novel pH-sensitive Salecan-g-poly(acrylic acid) hydrogel for controlled release of doxorubicin, *J Mater Chem B*, 3 (2015) 2685.

19 Tanwar M, Gupta R K & Rani A, Natural gums and their derivatives based hydrogels: In biomedical, environment, agriculture, and food industry, *Crit Rev Biotechnol*, 44 (2024) 275.

20 Küçükaşik F, Kazak H, Güney D, Finore I, Poli A, Yenigün O, Nicolaus B & Öner E T, Molasses as fermentation substrate for levan production by Halomonas sp., *Appl Microbiol Biotechnol*, 89 (2011) 1729.

21 Kucukasik F, Yenigun O & Toksoy O E, Molasses as fermentation substrate for microbial biopolymer production, *New Biotechnol*, 25 (2009) S250.

22 Fan M, Zhang S, Ye G, Zhang H & Xie J, Integrating sugarcane molasses into sequential cellulosic biofuel production based on SSF process of high solid loading, *Biotechnol Biofuels*, 11 (2018) 329.

23 Kumar D M & Gupta R K, Synthesis, characterization and application of Lignosulphonate-g- poly(sodium acrylate) hydrogel, *Indian J Chem Technol*, 30 (2023) 753.

24 Khaleghi M, Ahmadi E, Khodabandeh S M, Aliakbari F & Morshedi D, Temperature-dependent formulation of a hydrogel based on Hyaluronic acid-polydimethylsiloxane for biomedical applications, *Heliyon*, 6 (2020) e03494.

25 Srivastava A, Manu & Gupta R K, Xanthan Gum and lignin grafted chemically Crosslinked hydrogels for dye removal: Synthesis, characterization and isotherms studies, *Polym Sci Ser A*, 65 (2023) 725.

26 Manu, Kumar D & Gupta R K, Novel formulations of humic acid, lignin, and lignite grafted hydrogels for the slow release of thiamethoxam, *ChemistrySelect*, 9 (2024) e202304939.

27 Akalin G O & Pulat M, Controlled release behavior of zinc-loaded carboxymethyl cellulose and carrageenan hydrogels and their effects on wheatgrass growth, *J Polym Res*, 27 (2020) 1.

28 Tanwar M, Gupta R K & Rani A, Carboxymethylated gum tragacanth crosslinked poly(sodium acrylate)hydrogel: Fabrication, characterization, rheology and drug-delivery application, *Indian J Chem Technol*, 30 (2023) 308.

29 Rabat N E, Hashim S & Majid R A, Effect of different monomers on water retention properties of slow release fertilizer hydrogel, *Procedia Eng*, 148 (2016) 201.

30 Dharmalingam K & Anandalakshmi R, Fabrication, characterization and drug loading efficiency of citric acid crosslinked NaCMC-HPMC hydrogel films for wound healing drug delivery applications, *Int J Biol Macromol*, 134 (2019) 815.

31 Finkenstadt V L & Willett J L, Reactive extrusion of starch-polyacrylamide graft copolymers: Effects of monomer/starch ratio and moisture content, *Macromol Chem Phys*, 206 (2005) 1648.

32 Arndt K F, Richter A, Ludwig S, Zimmermann J, Kressler J, Kuckling D & Adler H J, Poly(vinyl alcohol)/poly(acrylic acid) hydrogels: FT-IR spectroscopic characterization of crosslinking reaction and work at transition point, *Acta Polym*, 50 (1999) 383.

33 Eisenberg A, Yokoyama T & Sambalido E, Dehydration kinetics and glass transition of poly(acrylic acid), *J Polym Sci Part A-1 Polym Chem*, 7 (1969) 1717.

34 Yu C, Wang F, Zhang C, Fu S & Lucia L A, The synthesis and absorption dynamics of a lignin-based hydrogel for remediation of cationic dye-contaminated effluent, *React Funct Polym*, 106 (2016) 137.

35 Reddy B V, & Rao G R, Vibrational spectra and modified valence force field for N,N'-methylenebisacrylamide, *Indian J Pure Appl Phys*, 46 (2008) 611.

36 Yadav R, Manu, Aayush & Rani A, Synthesis and characterization of xanthan gum and carboxymethylcellulose sodium salt based ionic crosslinked hydrogels for agricultural application, *Bulg Chem Commun*, 55 (2023) 131.

37 Ahmed I, Mahmood A, Qureshi O S, Sarfraz R M, Ijaz H, Zaman M, Akram M R, Usmani S, Zulcaif & Malook M, Development of tamarind gum/β-CD-co-poly (MAA) hydrogels for pH-driven controlled delivery of capecitabine, *Polym Bull*, 81 (2024) 6173.

38 Khan H, Yerramilli A S , D'Oliveira A, Alford T L, Boffito D C & Patience G S, Experimental methods in chemical engineering: X-ray diffraction spectroscopy - XRD, *Can J Chem Eng*, 98 (2020) 1255.

39 Santos F B, Miranda N T, Schiavon M I R B, Fregolente L V & Wolf Maciel M R, Thermal degradation kinetic of poly(acrylamide-co-sodium acrylate) hydrogel applying isoconversional methods, *J Therm Anal Calorim*, 146 (2021)2503.

40 Manu, Kumar D & Gupta R K, Harnessing lignite-based hydrogel for enhanced uv protection and delivery of dinotefuran in agriculture, *Polym Bull*, Vol (2024).page .

41 Stojkov G, Niyazov Z, Picchioni F & Bose R K, Relationship between structure and rheology of hydrogels for various applications, *Gels*, 7 (2021) 255.

42 Yadav R & Purwar R, Influence of metal oxide nanoparticles on morphological, structural, rheological and conductive properties of mulberry silk fibroin nanocomposite solutions, *Polym Test*, 93 (2021) 106916.

43 Murthy P S K, Mohan Y M, Sreeramulu J & Raju K M, Semi-IPNs of starch and poly(acrylamide-co-sodium methacrylate): Preparation, swelling and diffusion characteristics evaluation, *React Funct Polym*, 66 (2006) 1482.

44 Çaykara T & Turan E, Effect of the amount and type of the crosslinker on the swelling behavior of temperature-sensitive poly(N-tert-butylacrylamide-co-acrylamide) hydrogels, *Colloid Polym Sci*, 284 (2006) 1038.

45 Rajanna G A, Manna S, Singh A, Babu S, Singh V K, Dass A, Chakraborty D, Patanjali N, Chopra I, Banerjee T, Kumar A, Khandelwal A & Parmar B S, Biopolymeric superabsorbent hydrogels enhance crop and water productivity of soybean–wheat system in Indo-Gangetic plains of India, *Sci Rep*, 12 (2022) 11955.

46 Ahmed L, Atif R, Eldeen T S, Yahya I, Omara A & Eltayeb M, Study the using of nanoparticles as drug delivery system based on mathematical models for controlled release, *Int J Latest Technol Eng Manage Appl Sci*, 8 (2019) 52.

47 Ekenna I C & Abali S O, Comparison of the use of kinetic model plots and DD solver software to evaluate the drug release from griseofulvin tablets, *J Drug Deliv Ther*, 12 (2022) 5.

48 Paolino D, Tudose A, Celia C, Di-Marzio L, Cilurzo & Mircioiu C, Mathematical models as tools to predict the release kinetic of fluorescein from lyotropic colloidal liquid crystals, *Materials (Basel)*, 12 (2019) 693.

49 Dash S, Murthy P N, Nath L & Chowdhury P, Kinetic modeling on drug release from controlled drug delivery systems, *Acta Pol Pharm -Drug Res*, 67 (2010) 217.